Boron Hydrogen Compounds: Hydrogen Storage and Battery Applications

Hagemann, Hans-Rudolf

How to cite

HAGEMANN, Hans-Rudolf. Boron Hydrogen Compounds: Hydrogen Storage and Battery Applications. In: Molecules, 2021, vol. 26, n° 24, p. 7425. doi: 10.3390/molecules26247425

This publication URL: https://archive-ouverte.unige.ch/unige:157062
Publication DOI: 10.3390/molecules26247425

molecules

MDPI

Review

Boron Hydrogen Compounds: Hydrogen Storage and Battery Applications

Hans Hagemann

Département de Chimie Physique, Université de Genève, 30, Quai E. Ansermet, CH1211 Geneva 4, Switzerland; hans-rudolf.hagemann@unige.ch

Abstract: About 25 years ago, Bogdanovic and Schwickardi (B. Bogdanovic, M. Schwickardi: *J. Alloys Compd*. 1–9, 253 (1997) discovered the catalyzed release of hydrogen from $NaAlH_4$. This discovery stimulated a vast research effort on light hydrides as hydrogen storage materials, in particular boron hydrogen compounds. $Mg(BH_4)_2$, with a hydrogen content of 14.9 wt %, has been extensively studied, and recent results shed new light on intermediate species formed during dehydrogenation. The chemistry of $B_3H_8^-$, which is an important intermediate between BH_4^- and $B_{12}H_{12}^{2-}$, is presented in detail. The discovery of high ionic conductivity in the high-temperature phases of $LiBH_4$ and $Na_2B_{12}H_{12}$ opened a new research direction. The high chemical and electrochemical stability of *closo*-hydroborates has stimulated new research for their applications in batteries. Very recently, an all-solid-state 4 V Na battery prototype using a $Na_4(CB_{11}H_{12})_2(B_{12}H_{12})$ solid electrolyte has been demonstrated. In this review, we present the current knowledge of possible reaction pathways involved in the successive hydrogen release reactions from BH_4^- to $B_{12}H_{12}^{2-}$, and a discussion of relevant necessary properties for high-ionic-conduction materials.

Keywords: boron hydrides; hydrogen storage; solid ionic conductors

Citation: Hagemann, H. Boron Hydrogen Compounds: Hydrogen Storage and Battery Applications. *Molecules* **2021**, *26*, 7425. https://doi.org/10.3390/molecules26247425

Academic Editors: Andrea Rossin, Igor Golub and Vladimir Bregadze

Received: 15 October 2021
Accepted: 2 December 2021
Published: 7 December 2021

1. Introduction

Boron hydrogen compounds have been intensively studied for almost a century since the pioneering studies of A. Stock [1]. Boron hydrogen compounds are also energetic materials and were considered as rocket or jet fuels [2]; however, the toxicity of boranes has prevented their extended use. Currently, nontoxic compounds such as ammonia-borane are also studied as hypergolic propellants [3,4]. Recently, many different applications of boron hydrogen compounds have emerged [5]. In particular, compounds derived from *closo*-hydroborates such as $B_{12}H_{12}^{2-}$ have found many new applications, including new all-solid-state batteries, medical applications, and as catalysts [6–11]. Since the discovery of catalyzed hydrogen release in $NaAlH_4$ by Bogdanovic and Schwickardi [12], light boron and aluminum hydrides were intensively studied and reviewed as potential hydrogen storage materials [13–22]. The dehydrogenation reactions of metal borohydrides ultimately lead to hydrogen, metal and boron, or metal borides. In this reaction process, intermediate species are formed, particularly compounds with *closo*-hydroborate anion $B_{12}H_{12}^{2-}$ [23,24]. $B_{12}H_{12}^{2-}$ is particularly stable and can thus also act as a detrimental thermodynamic sink for further dehydrogenation reactions. The properties of *closo*-hydroborates and related anions were addressed in several recent publications [6,25–28]. New research on the thermal properties of *closo*-hydroborate salts revealed a high-temperature phase transition in $Na_2B_{12}H_{12}$ leading to a superionic phase [29]. Thus, the controlled dehydrogenation of a borohydride salt can be used to safely prepare new *closo*- and *nido*- hydroborate salts for potential battery applications [30] without using toxic boranes such as $B_{10}H_{14}$, which were used for the synthesis of this large boron species [31].

In this review, we first describe experimental results on hydrogen storage in $Mg(BH_4)_2$, which has a large hydrogen content of 14.9 wt %. Hydrogen storage in other borohydrides, such as $LiBH_4$, was recently reviewed [32]. Recent results on potential dehydrogenation

intermediates for $Mg(BH_4)_2$ provide new insights on the potential reaction intermediates and are reported here. In this context, we then present recent results based on DFT calculations to explore possible reaction paths for successive dehydrogenation reactions starting from BH_4^-. These paths are described in more detail in the following section, which discusses the formation and reactions of $B_3H_8^-$, as this ion is considered to be one of the reaction intermediates during the dehydrogenation of borohydride compounds. The high-temperature dehydrogenation of $B_3H_8^-$ leads to the formation of *closo*-hydroborate anions $B_{10}H_{10}^{2-}$ and $B_{12}H_{12}^{2-}$, which form excellent solid ionic conductors for new all-solid-state batteries [30]. The properties of these ionic conductors are presented in the last section.

2. Magnesium Borohydride

Among the many compounds considered for hydrogen storage, $Mg(BH_4)_2$ is particularly interesting and has been studied by many authors. The earlier studies on $Mg(BH_4)_2$ were reviewed in detail in 2016 [22]. $Mg(BH_4)_2$ has a hydrogen content of 14.9 mass % [22,33]. This compound can be prepared in different crystalline modifications, and high pressure-phase transitions were also observed [33]. Porous γ-$Mg(BH_4)_2$ can also adsorb 0.8 H_2 at low temperatures and 100 bar to achieve a total hydrogen mass content of 17.4% [33]. High-pressure phase δ-$Mg(BH_4)_2$ has a very high volumetric hydrogen content of 147 g H_2/L. $Mg(BH_4)_2$ can also form amorphous solids. Overall dehydrogenation reaction

$$Mg(BH_4)_2 \rightarrow MgB_2 + 4\ H_2$$

is, in fact, a multistep reaction (see Figure 1) with various reaction intermediates, such as $Mg(B_3H_8)_2$, MgH_2, and $MgB_{12}H_{12}$, which were proposed both experimentally and theoretically [22,34–36]. MgB_2 is the decomposition product obtained after heating to 500 °C [37]. Boron-rich MgB_7 films are obtained by heating volatile $Mg(B_3H_8)_2$ solvates with dimethyl ether and diethyl ether [38].

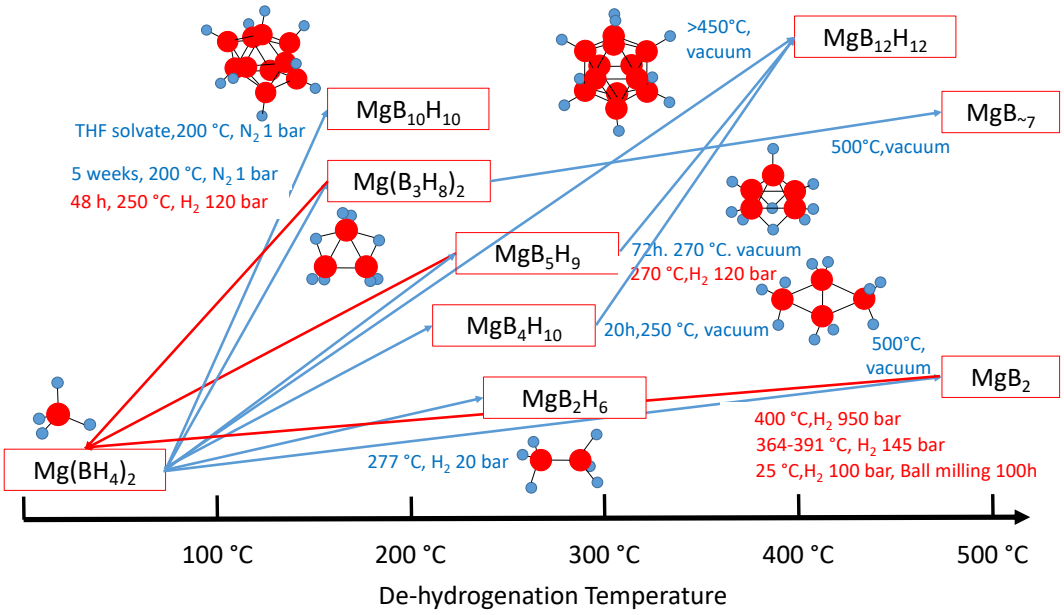

Figure 1. Illustration of $Mg(BH_4)_2$ dehydrogenation reactions (blue arrows) and rehydrogenation reactions (red arrows) reported in the literature [22,34–44]. Upon further heating, these intermediate species, which are associated with (amorphous) MgH_2, form MgB_2.

MgB_2 can be rehydrogenated, although under drastic conditions (950 bar H_2 at 400 °C) [40]. The rehydrogenation of MgB_2 can be accelerated with THF, MgH_2, and Mg [41]. Mechanically milled mixtures of MgB_2, THF, and 40 mol % Mg could thus ab-

sorb 6 wt % of H_2 at 300 °C under 700 bar of H_2, which is less drastic than that without THF. Recently, rehydrogenation at room temperature with mechanical activation by ball milling was reported [42]. These rehydrogenation reactions of MgB_2 demonstrate the principle that hydrogen storage in $Mg(BH_4)_2$ is indeed reversible. A recent combined experimental and theoretical study concluded that the initial stages of rehydrogenation are associated with the formation of σ bonds of hydrogen with boron on the reactive edges of the MgB_2 solid [43]. The rehydrogenation of intermediate compounds was also studied. MgB_3H_8.THF can be rehydrogenated under milder conditions than those of dry MgB_3H_8 (50 bar H_2 and 200 °C for 5 h vs. 120 bar H_2 and 250 °C for 48 h) [44]. MgH_2 is formed in intermediate reaction steps, such as

$$6\ Mg(BH_4)_2 \rightarrow\ MgB_{12}H_{12} + 5\ MgH_2 + 13\ H_2$$

Magnesium hydride dissociates into Mg and H_2 at high temperatures and low H_2 pressures. The different reaction products observed under various conditions (see Figure 1) show that the reaction kinetics can be influenced by various parameters, which also include the initial crystalline modification of $Mg(BH_4)_2$.

The overall enthalpy of reaction for the dehydrogenation of $Mg(BH_4)_2$ ($\Delta_fH°$ = −208 kJ/mol) to form MgB_2 ($\Delta_fH°$ = −91.96 kJ/mol) and hydrogen can be calculated [45–47] to be equal to +116 kJ/mol, i.e., less than 30 kJ/mol per hydrogen molecule released, which is, in principle, in the correct range for a hydrogen storage material [13]. The first step of a dehydrogenation reaction of BH_4^- is likely to be the breaking of a B–H bond. Isotope exchange reactions of $Mg(BH_4)_2$ with D_2 allow for producing a complete exchange to form $Mg(BD_4)_2$, and the corresponding activation energy was estimated to be about 51 kJ/mol [48]. For $Ca(BH_4)_2$, the corresponding activation energy was found to be 82 and 98.5 kJ/mol for the reverse reaction, confirming that breaking a bond with hydrogen or deuterium is the rate-limiting step [49]. Theoretical calculations of potential defects in $Mg(BH_4)_2$ suggest that, in the initial phase of the dehydrogenation, a H^- ion is formed that can diffuse in the lattice [50]. On the other hand, gas diffusion in the solid is also a contribution to exchange kinetics, as was shown by isotope exchange reactions with the highly porous modification of γ-$Mg(BH_4)_2$ with a high surface area compared to a ball-milled sample with a strongly reduced surface aera [51].

The reaction kinetics of hydrogen release in $Mg(BH_4)_2$ can be significantly enhanced by various additives, such as $TiCl_3$ [52] or NbF_5 and TiO_2 [53]. Lewis bases in the form of solvates of $Mg(BH_4)_2$ can also accelerate the hydrogen release [54]. As shown in Figure 1, the THF solvate releases H_2 gas below 200 °C to form $Mg(B_{10}H_{10})$. The formation of $B_3H_8^-$ and $B_{12}H_{12}^{2-}$ was also observed, but with THF and dimethyl ether, $B_{12}H_{12}^{2-}$ remained a minor reaction product. The physical properties of $Mg(BH_4)_2$.3THF were recently investigated in detail [55]. In this compound, Mg^{2+} is coordinated to 2 BH_4^- ions and 3 THF molecules. The orientational mobilities of the BH_4^- ions are not particularly sensitive to the presence of THF. The authors concluded that "the presence of THF also disrupts the stability of the crystalline phase leading to enhanced kinetics for the dehydrogenations". Recently, Tran et al. [56] reported that the presence of different glymes with $Mg(BH_4)_2$ results in various ratios of $MgB_{10}H_{10}$ and $MgB_{12}H_{12}$ upon thermolysis at 160–200 °C, and allows for selectively obtaining $MgB_{10}H_{10}$ with one equivalent of monoglyme. Mixtures of $Mg(BH_4)_2$ with $(CH_3)_4NBH_4$ (5:1 molar) reveal reversible melting around 180–195 °C [57] with enhanced stability compared to melts of pure $Mg(BH_4)_2$ and $(CH_3)_4NBH_4$. $[Ph_4P]_2[Mg(BH_4)_4]$ gradually loses mass over 225–230 °C, but heating to 500 °C does not lead to the mass loss expected for the formation of MgB_2. A similar behavior was observed for $[Me_4N]_2[Mg(BH_4)_4]$ [58]. These findings suggest that derivates of $Mg(BH_4)_2$ with organic cations are rather stabilized.

Solvent-free $Mg(B_3H_8)_2$ can be prepared by ball milling $MgBr_2$ with NaB_3H_8 [38,59]. Kim et al. [38] reported the formation of boron-rich MgB_7 films upon heating under vacuum above 425 °C due to some evaporation of Mg under these conditions. Thermogravimetry (TG) experiments [59] revealed a 30 wt % mass loss setting in above ca 80 °C corresponding to the evolution of B_2H_6, B_5H_9 and H_2. The residual solid after heating to 200 °C was a

mixture of mainly $Mg(BH_4)_2$, $Mg(B_{10}H_{10})$, and $Mg(B_{12}H_{12})$, and the combined evolution of H_2, B_2H_6, and B_5H_9 was confirmed by mass spectrometry [60]. The addition of activated (ball-milled) MgH_2 to $Mg(B_3H_8)_2$ results in a strong reduction in borane evolution and up to 88% conversion back to $Mg(BH_4)_2$ at 100 °C. The presence of activated MgH_2 thus substantially decreases the formation of (*closo*-hydro)borates and provides the necessary hydrogen for the conversion of $B_3H_8^-$ back into BH_4^-.

These experiments suggest that, while Lewis acids may favor the dehydrogenation reactions of $Mg(BH_4)_2$, they do not necessarily catalyze the rehydrogenation reactions, as transition metal halides do not appear to affect the rehydrogenation of MgB_2 [40,61]. THF and other Lewis bases appear to accelerate both the dehydrogenation and rehydrogenation reactions of $Mg(BH_4)_2$, and encourage more studies to even further improve the kinetics.

3. DFT Calculations

The results presented above for $Mg(BH_4)_2$ suggest the formation of various intermediate species such as $B_2H_6^{2-}$, $B_3H_8^-$, $B_4H_{10}^{2-}$, $B_5H_9^{2-}$ and the *closo*-borates $B_nH_n^{2-}$ (n = 8–12). For hydrogen storage applications, the only gaseous species resulting from dehydrogenation reactions should be hydrogen; thus, neutral boranes are a priori not involved in the reaction mechanisms. Many other anionic boron hydrides have been reported in the literature and could be involved in one reaction step or another. In 1999, some reactions between neutral and anionic boron hydrides related to the formation of $B_3H_8^-$, B_5 anions, and some other species were reviewed [62].

In order to assess the driving forces for different reactions, thermodynamic information can be very useful, but experimental data are very scarce. For alkali borohydrides, thermodynamical data are available [47], but only few other experimental data are available. Using the experimental values of the formation enthalpy of $Mg(BH_4)_2$ [45] and $La(BH_4)_3$ [63], the formation enthalpy of other $M(BH_4)_2$ and $M(BH_4)_3$ compounds were estimated, assuming that the lattice enthalpy of bromides and borohydrides with the same metal ion were identical within about 15 kJ/mol [46]. The experimental formation enthalpy of $NH_4B_3H_8$ (-530 ± 33 kJ/mol) [64], $(NH_4)_2B_{10}H_{10}$ (-359.2 ± 10 kJ/mol) [65], and of guanidinium and other nitrogen-based *closo*-borates was reported [66]. Recently, new heat capacity measurements for Na, K, Rb, Cs, Mg, Ca borohydrides were reported [67]. The knowledge of all thermodynamic properties in principle allows for quantitatively describing the phase diagram of a system, which was performed using available data for the Mg–B–H system [68].

In the absence of experimental data, theoretical data are obtained. It is quite challenging to obtain accurate results of formation enthalpies using DFT. Nguyen et al. [69] calculated for the formation enthalpy of $(NH_4)_2B_{10}H_{10}$ with the G3 method the value of -184 kJ/mol, which is quite different from the experimental value of -359.2 kJ/mol. For α-$Mg(BH_4)_2$, formation enthalpy values ranging from -67 to -277 kJ/mol were reported in the literature [68], while the experimental value was -208 kJ/mol [45]. Zhang et al. [23] computed relative formation energies of potential solid intermediates formed during the dehydrogenation of $Mg(BH_4)_2$, in combination with a Monte Carlo-based structure prediction method. They predicted a potential $Mg_3(B_3H_6)_2$ intermediate with a $B_3H_6^{3-}$ ion, while $Mg(B_3H_8)_2$ was found to be very high in relative energy and thereby unlikely to be formed.

The principal difficulty for estimating the formation enthalpy of crystalline solids is the evaluation of lattice energy, as different approaches (volume-based, Kaputinski equation etc.) lead to different values. Further, lattice energies can only be computed for crystalline materials, preferentially on the basis of experimental structure data, but experiments showed that a significant fraction of the reaction intermediates remain amorphous, complicating things even further.

DFT calculations in the gas phase are quite reliable, and allow for obtaining good structural data and vibrational frequencies, in particular when anharmonicity is included. Several studies report the formation enthalpy of borohydride ions in the gas phase [69–72]

Anharmonic DFT calculations allow for obtaining improved agreement with experimental vibrational spectra, from which heat capacity data were calculated [73]. Figure 2 compares experimental [74] and DFT calculated [69–72] formation enthalpy data for neutral and anionic boron hydrogen species. Figure 2 shows that the calculated formation enthalpy for a given species (e.g., $B_3H_8^-$) can differ by about 100 kJ/mole for different sources. These values are derived, for instance, from isodesmic reactions with known formation heat [69], thus generating a potential propagation of errors if the initial formation enthalpy values are different. We outline all reported values to highlight the limitations of the accuracy of these data.

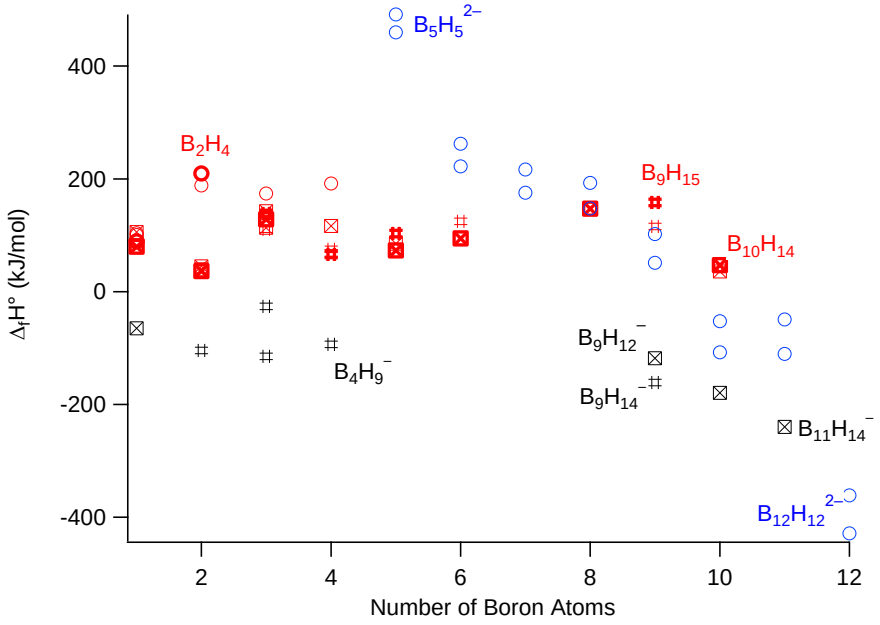

Figure 2. Experimental (bold) and theoretical formation enthalpy values for neutral (red) monoanionic (black) and dianionic (blue) species. *Closo* species, circles; *nido*, #; *arachno*, crossed squares. Data from [69–72,74–76]. For *closo* ions $B_nH_n^{2-}$, data (blue circles) from 2 different studies [69,72] reveal systematic differences. All monoanionic species (in black) have negative formation enthalpies, while all neutral boranes (in red) have positive formation enthalpy.

Figure 2 shows that the experimental formation enthalpies of neutral species are all positive [74], with values ranging from 36 kJ/mol (for B_2H_6) to 210 kJ/mol for (B_2H_4). Gas phase reaction

$$2\ B_2H_6 \rightarrow\ B_4H_{10} + H_2$$

has an enthalpy change of $66.1 - 2 \times 36.4 = -6.7$ kJ/mol, and shows that increasing the number of boron atoms in the cluster can be thermodynamically favorable for neutral species. Other reactions towards larger hydroboranes may become favorable at higher temperatures from the liberation of hydrogen. The first theoretical studies of enthalpy changes for reactions of neutral boranes were reported by M.L. McKee in 1990 [70], who showed that a sequence of BH_3 additions followed by H_2 elimination from B_2H_6 to B_6H_{10} is overall exothermic, but with two less stable reaction intermediates (B_3H_9 and B_4H_8) that can act as barrier steps for the kinetics. Figure 2 shows that anionic species with 9–12 boron atoms are the most stable, which indicates that there is a thermodynamic driving force towards these anions. The most stable species in this figure is the *closo* $B_{12}H_{12}^{2-}$ ion, and its stability is related to its 3-dimensional aromaticity [6]. The formation enthalpy of $B_{12}H_{12}^{2-}$ in the gas phase was estimated to be between -325.5 and -428.6 kJ/mol according to different theoretical studies [72,75,76]. One key intermediate in the overall dehydrogenation reactions of BH_4^- appears to be ion $B_3H_8^-$, which is discussed in the next section.

4. Formation and Reactions of $B_3H_8^-$

As mentioned above, the formation of $Mg(B_3H_8)_2$ was observed during the decomposition of $Mg(BH_4)_2$ under dynamic vacuum [54,77], and $Y(B_3H_8)_3$ was obtained after heating $Y(BH_4)_3$ under hydrogen pressure of 1–10 bar [78]. There are several reports in the literature on the synthesis of $B_3H_8^-$ that highlight that various routes can lead to this ion. Starting from diborane under strongly reducing conditions, dianion $B_2H_6^{2-}$ was reported to form [62,79]

$$2\ B_2H_6 + 2\ C_8H_{10}^- \rightarrow\ [BH_3^{2-}] + BH_3 + 2\ C_8H_{10} \rightarrow\ [B_2H_6^{2-}] + 2\ C_8H_{10}$$

BH_3^{2-} and $B_2H_6^{2-}$ intermediates were identified by NMR. The reaction of $B_2H_6^{2-}$ with additional diborane yields $B_3H_8^-$ + BH_4^-, and no further intermediate was observed:

$$B_2H_6 + B_2H_6^{2-} \rightarrow\ B_3H_8^- + BH_4^-$$

Another reaction observed was the reaction of potassium metal with $THF.BH_3$ [80].

$$2\ K + 4\ THF.BH_3 \rightarrow\ 2\ K^+ + B_3H_8^- + BH_4^-$$

Beall and Gaines [62] argue that also in this case, $B_2H_6^{2-}$ is the reaction intermediate, which can then react with THF–BH_3 to form either $B_2H_5^-$ + BH_4^- with the addition of the 4th $THF.BH_3$ $B_3H_8^-$ or first with THF–BH_3 the ion $B_3H_9^{2-}$, which then reacts with $THF.BH_3$ to yield $B_3H_8^-$ + BH_4^-. $B_3H_8^-$ can also be formed from the reaction of BH_4^- with diborane [81]:

$$BH_4^- + B_2H_6 \rightarrow\ B_3H_8^- + H_2$$

$$BH_4^- + B_2H_6 \rightarrow\ BH_3 + B_2H_7^- \rightarrow\ BH_3 + B_2H_5^- + H_2 \rightarrow\ B_3H_8^- + H_2$$

$$BH_4^- + B_2H_6 \rightarrow\ BH_3 + B_2H_7^- \rightarrow\ B_3H_{10}^- \rightarrow\ B_3H_8^- + H_2$$

This reaction can proceed either via $B_2H_7^-$ (hydride transfer) and $B_3H_{10}^-$ (BH_3 addition) followed by H_2 detachment or via $B_2H_7^-$, which first loses H_2 to form $B_2H_5^-$, which then adds BH_3. The efficient synthesis of alkali metal octahydrotriborates (M = Na, K, Rb, Cs) from the reaction of MBH_4 with 2 equivalents of dimethyl sulfide borane was reported [82]. The formation of ion $B_2H_7^-$ was observed by NMR for the reaction of $LiBH_4$ with $THF.BH_3$ in THF [83], and during the solvothermal reaction of BH_4^- with CH_2Cl_2 at 70 °C [84]. The reaction of BD_4^- requires higher temperatures (90 °C) [84], which suggests that the rate-determining reaction step is associated with the breaking of a boron–hydrogen (deuterium) bond, which could be the formation of a reactive Lewis adduct of BH_3 from BH_4^-, which then reacts with other BH_4^- to form $B_2H_7^-$ etc., as outlined above.

Once formed, $B_3H_8^-$ can further react to yield B_9 to B_{12} hydroborate anions. Using the DFT calculation formation enthalpies of $B_9H_{14}^-$, $B_3H_8^-$ and BH_4^- [71], for the gas phase reactions, one obtains

$$4\ B_3H_8^- \rightarrow\ B_9H_{14}^- + 3\ BH_4^- + 3\ H_2$$

$$4\ B_3H_8^- \rightarrow\ B_{10}H_{10}^{2-} + 2\ BH_4^- + 9\ H_2$$

exothermic reaction enthalpy values of −413 and −49.8 kJ/mol, respectively, and a strong entropy increase that even further favors the reaction at higher temperatures. These spontaneous overall reaction enthalpies also explain why potential reaction intermediates with 6 to 8 boron atoms are practically not observed. The simultaneous production of BH_4^- in these reactions adds a thermodynamic driving force (as the formation enthalpy of BH_4^- is negative) for these reactions.

In the presence of hydrides, Grinderslev et al. [85] observed the following decomposition reaction at 150 and 200 °C of KB_3H_8 under 380 bar of H_2:

$$KB_3H_8 + 2KH \rightarrow\ KBH_4 + K_2B_{12}H_{12} + K_2B_{10}H_{10} + K_2B_9H_9$$

As shown above, heating solvent-free $Mg(B_3H_8)_2$ + 4 MgH_2 either with or without H_2 gas results in up to 88% back conversion to $Mg(BH_4)_2$ with some $MgB_{12}H_{12}$ [60]. These results show that $B_3H_8^-$ can react in many different ways to either form larger boron hydride clusters or regenerate BH_4^-. This can be exploited, for instance, to achieve the direct synthesis of $B_{10}H_{10}^{2-}$ and $B_{12}H_{12}^{2-}$ to prepare solid ionic conductors such as $Na_4(B_{10}H_{10})(B_{12}H_{12})$, as demonstrated by Gigante et al. [86]. This synthesis starts with the conversion of $NaBH_4$ into $(Et_4N)BH_4$, which reacts solvothermally with CH_2Cl_2 to form $(Et_4N)B_3H_8$. $(Et_4N)B_3H_8$ is then heated in toluene to 185 °C to form a mixture of $(Et_4N)_2B_{10}H_{10}$ and $(Et_4N)_2B_{12}H_{12}$, which can then either be separated by fractional crystallization or directly converted with sodium tetraphenylborate into ionic conductor $Na_4(B_{10}H_{10})(B_{12}H_{12})$.

5. Closoborates and Related Species as Solid Ionic Conductors

Solid ionic conductors for lithium or sodium batteries allow for avoiding the use of a flammable organic electrolyte and are thus expected to considerably improve the safety of batteries. A good solid electrolyte must fulfill several empirical criteria, according to [87]:

- "open structure" with a low coordination number of the mobile ion;
- The presence of structural phase transitions at low pressure. In the case of AgI, the ambient pressure wurtzite structure (space group $P6_3mc$) transforms at 3 kbar and 315 K into a NaCl structure (space group Fm-3m), thus going from a rather covalent network with coordination number 4 to a rather ionic structure with coordination number 6. The associated charge fluctuations between ions can potentially be coupled to vibrational motions and thus dynamically favor ionic conduction.

For practical applications, the conductivity of the material should be higher than 1 mS/cm. Further, the material should have high chemical and thermal stability, and a high electrochemical stability window. Additionally, it must be electronically insulating to avoid battery self-discharge or shortage. Further, the electrolyte should be deformable in order to accommodate the volume changes of anode and cathode materials upon lithium or sodium insertion and removal. This can thus limit the formation of fractures that reduce the performance of the battery. Lastly, the material should not be toxic and be cheap enough for the considered applications.

The discovery of superionic conductivity in the high-temperature phases of $LiBH_4$ [88] and $Na_2B_{12}H_{12}$ [29] has stimulated new research for similar compounds with high ionic conductivity at lower temperatures. These compounds include *closo*-hydroborates, *nido*-hydroborates ($B_{11}H_{14}^-$), and *closo*-hydrocarborates ($CB_9H_{10}^-$, $CB_{11}H_{12}^-$). Ions $B_{10}H_{10}^{2-}$ and $B_{12}H_{12}^{2-}$ are not very toxic. Mutterties et al. [89] reported LD_{50} values for $Na_2B_{10}H_{10}$ and $Na_2B_{12}H_{12}$ administered orally to rats to be around or higher than 7.5 g/kg of body weight for both compounds.

The crystal chemistry of inorganic hydroborates except BH_4^- was recently presented in detail [90], while the crystal chemistry of salts with BH_4^- was addressed in an earlier review [18]: "All nonmolecular hydroborate crystal structures can be derived by simple deformation of the close-packed anionic lattices, i.e., cubic close packing (ccp) and hexagonal close packing (hcp), or bodycentered cubic (bcc), by filling tetrahedral or octahedral sites" [90]. This observation can be illustrated considering group–subgroup relationships of encountered crystal structures, as illustrated in Figure 3 for some relevant compounds [90–102]. Crystal packing is governed by large anions, leaving in some space groups empty cationic sites, which, of course, favor ionic conduction. For instance, β-$Na_2B_{12}H_{12}$ crystallizes in the Pm-3n space group with a statistical population of 6 sites occupied by 4 Na^+ ions.

Perturbations of the anionic sublattice further allow for stabilizing the conductive phase at lower temperatures. This was first demonstrated for solid solutions of $LiBH_4$ with LiBr and LiI [103]. Phase stability and ionic conductivity in mixed $LiBH_4$–LiX (X = Cl, Br) was recently studied in detail [104]. Perturbations of the structure by ball milling or partial substitution was demonstrated for $Na_2B_{12}H_{12}$ with a partial introduction of iodine ions in the *closo*-hydroborate [105]. In a further step, solid solutions of *closo*-hydroborate and

closo-carbahydroborates, and solid solutions of *nido*-hydroborates with *closo*-hydroborates were studied [106–112]. Representative examples of mixed borate ionic conductors are shown in Table 1.

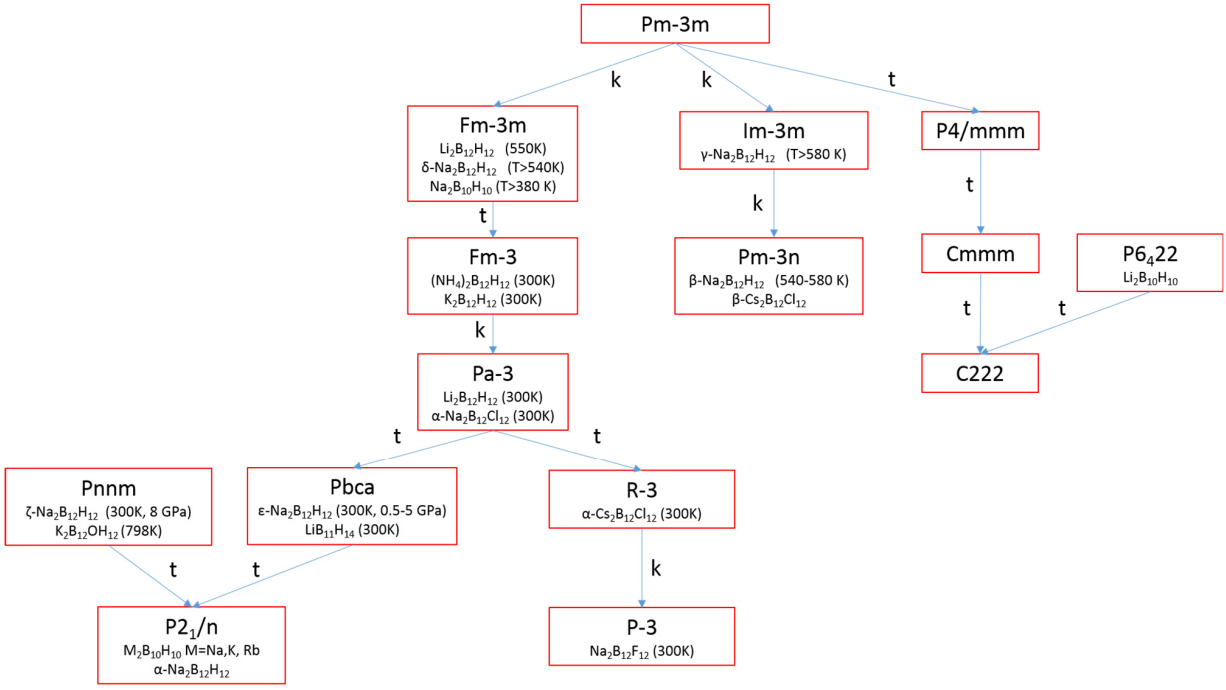

Figure 3. Group–subgroup relationships between space groups (in Herrmann-Mauguin notation) of *closo*-hydro borates and some *closo*-halogeno borates. t, "translationengleich" subgroups; k, "klassengleich" subgroups.

Table 1. Examples of ionic conductivity in mixed borate salts.

Compound	Temperature	Conductivity	Reference
0.7 $Li(CB_9H_{10})$–0.3 $Li(CB_{11}H_{12})$	298 K	6.7 mS/cm	[106]
$Li_2(B_{11}H_{14})(CB_{11}H_{12})$	298 K	0.11 mS/cm	[107]
$Li_3(B_{11}H_{14})(CB_{11}H_{12})_2$	298 K	1.1 mS/cm	[107]
$Na_3(CB_{11}H_{12})(B_{12}H_{12})$	298 K	2 mS/cm	[108]
$Na_4(CB_{11}H_{12})_2(B_{12}H_{12})$	298 K	2 mS/cm	[108]
$Na_4(B_{10}H_{10})(B_{12}H_{12})$	298 K	0.9 mS/cm	[109]
$Na_2(B_{10}H_{10})-3\ Na_2(B_{12}H_{12})$	298 K	0.34 mS/cm	[110]
$Na_{x+2y}(B_{11}H_{14})_x(B_{12}H_{12})_y$	298 K	3–4 mS/cm	[111]

The mechanism of ionic conduction in these compounds is related to the dynamical properties of the borohydride or carbohydride ions. These properties can be addressed using NMR [113] and neutron techniques [114], in conjunction with temperature-dependent conductivity and X-ray diffraction, and are supported by theoretical calculations [76,77,88]. A detailed study of ionic conductor $Na_4(B_{12}H_{12})(B_{10}H_{10})$ [115] with all these techniques revealed 3 different regimes with increasing temperature. Below −50 °C, conductivity remains very low. Above this temperature, an apparent activation energy of 0.6 eV was found, related to significant couplings of anionic and cationic motions. Above 70 °C, activation energy decreases to 0.37 eV, as thermal energy leads to noncorrelated ionic motions.

One important aspect of solid ionic conductors is their electrochemical stability, which is a critical limit for a reversible battery application. Asakura et al. [116] developed a linear sweep voltammetry method to reliably measure the electrochemical stability of borohydride-based solid electrolytes. The measured oxidative stability of $LiBH_4$ of 2.0 V

vs. Li^+/Li was significantly smaller than that in initial reports claiming a stability of up to 5 V [117]. For $Na_4(B_{12}H_{12})(B_{10}H_{10})$, two oxidation onsets at 3.02 and 3.22 V vs. Na^+/Na were tentatively assigned to the onset of decomposition of the less stable $[B_{10}H_{10}]^{2-}$ and more stable $[B_{12}H_{12}]^{2-}$ ions, respectively [116]. *Closo*-carborane ions are even more stable, as for $Na_4(CB_{11}H_{12})_2(B_{12}H_{12})$, where a large anodic current was observed above 4 V vs. Na^+/Na, together with a small onset at 2.93 V. For $Li_2(CB_9H_{10})(CB_{11}H_{12})$, the onset of decomposition was observed at 2.86 V vs. Li^+/Li [116]. *Nido*-borates are electrochemically less stable. The oxidative stability limit for $Na_5(B_{11}H_{14})(B_{12}H_{12})_2$ was 2.6 V vs. Na^+/Na, and for $LiB_{11}H_{14}$, 2.6 V vs. Li^+/Li [107].

These developments have also led to several all-solid-state battery prototypes based on these mixed borate ionic conductors. Duchêne et al. [118] presented a 3 V sodium battery using $Na_4(B_{12}H_{12})(B_{10}H_{10})$, and Murgia et al. [119] showed Na stripping/plating over >500 h in a Na cell with $Na_4(CB_{11}H_{12})_2(B_{12}H_{12})$. Recently, Asakura et al. [120] demonstrated a 4 V sodium battery with the same solid-state conductor, $Na_4(CB_{11}H_{12})_2(B_{12}H_{12})$. These results show that *closo*-hydroborates and their derivatives are very promising materials for chemically and electrochemically stable all-solid-state ionic conductors.

6. Conclusions

In the last 20 years, many studies on borohydride species have considerably increased our knowledge on the properties of these materials. For hydrogen storage applications, the kinetics and reversibility of the dehydrogenation reactions remain a major challenge for practical applications. The chemistry of borohydrides from BH_4^- to $B_{12}H_{12}^{2-}$ in the gas phase and in solution has been theoretically and experimentally addressed; however, in solids, these studies are very challenging, as structural data of potential reaction intermediates such as $Mg(B_3H_8)_2$ are elusive, and not all intermediates can be observed. If the reaction intermediates are amorphous, X-ray diffraction cannot be used, and theoretical approaches can lead to many different potential structures. The presence of additional hydrides or of Lewis bases such as THF, as shown for the reactions of KB_3H_8 and $Mg(B_3H_8)_2$, strongly modifies the reaction products upon heating. We are thus still very far from a full microscopic understanding of these hydrogenation–dehydrogenation reactions and in the search for optimal catalysts for these processes.

For hydrogen storage, $B_3H_8^-$ is an interesting species that can be rehydrogenated back to BH_4^-. Even though only 25% of the hydrogen is available for this reversible hydrogen storage, the temperatures (less than 200 °C) and kinetics of these reactions approach practical conditions.

The *closo*-hydroborate ions that are formed and identified as intermediates of dehydrogenation reactions have found new and very promising applications as solid-state ionic conductors, as they present many very favorable properties for this use. The recent demonstration of a 4 V all-solid-state battery using solid sodium electrolyte $Na_4(CB_{11}H_{12})_2(B_{12}H_{12})$ [120] highlights this potential. Whether compounds such as $Mg(B_{10}H_{10})$, which can be obtained starting from $Mg(BH_4)_2.2THF$, are applicable for new Mg-based batteries remains to be demonstrated. In the preparation of these *closo*-hydroborates and their derivatives, starting from BH_4^- instead of neutral boranes, has the great advantage to reduce the toxicity of the reactants. B_2H_6, B_5H_9 and $B_{10}H_{14}$ are highly toxic and thereby not really suitable for industrial production processes of *closo*-hydroborates at a higher scale. Thus, boron–hydrogen compounds have a future for new green energy applications.

Funding: This research was funded by the Swiss National Science Foundation, grant number 200020_182494.

Institutional Review Board Statement: Not applicable.

Informed Consent Statement: Not applicable.

Data Availability Statement: Not applicable.

Conflicts of Interest: The author declares no conflict of interest.

References

1. Stock, A. *The Hydrides of Boron and Silicon*; Cornell University Press: New York, NY, USA, 1933.
2. Martin, D.R. The Development of Borane Fuels. *J. Chem. Educ.* **1959**, *36*, 208–214. [CrossRef]
3. Baier, M.J.; Veeraraghavan Ramachandran, P.; Son, S.F. Characterization of the Hypergolic Ignition Delay of Ammonia Borane. *J. Propuls. Power* **2019**, *35*, 182–189. [CrossRef]
4. Zhang, Z.; Zhao, Z.; Wang, B.; Zhang, J. Boron based hypergolic ionic liquids: A review. *Green Energy Environ.* **2020**, *6*, 794–822. [CrossRef]
5. Huang, Z.; Wang, S.; Dewhurst, R.D.; Ignat'ev, N.V.; Finze, M.; Braunschweig, H. Boron: Its Role in Energy-Related Processes and Applications. *Angew. Chem. Int. Ed.* **2020**, *59*, 8800–8816. [CrossRef]
6. Zhao, X.; Yang, Z.; Chen, H.; Wang, Z.; Zhou, X.; Zhang, H. Progress in three-dimensional aromatic-like closo-dodecaborate. *Coord. Chem. Rev.* **2021**, *444*, 214042. [CrossRef]
7. Stauber, J.M.; Schwan, J.; Zhang, X.; Axtell, J.C.; Jung, D.; McNicholas, B.J.; Oyala, P.H.; Martinolich, A.J.; Winkler, J.R.; See, K.A.; et al. A Super-Oxidized Radical Cationic Icosahedral Boron Cluster. *J. Am. Chem. Soc.* **2020**, *142*, 12948–12953. [CrossRef]
8. Tu, D.; Yan, H.; Poater, J.; Solà, M. The nido-Cage···π Bond: A Non-covalent Interaction between Boron Clusters and Aromatic Rings and Its Applications. *Angew. Chemie Int. Ed.* **2020**, *59*, 9018–9025. [CrossRef] [PubMed]
9. Alamón, C.; Dávila, B.; García, M.F.; Sánchez, C.; Kovacs, M.; Trias, E.; Barbeito, L.; Gabay, M.; Zeineh, N.; Gavish, M.; et al. Sunitinib-Containing Carborane Pharmacophore with the Ability to Inhibit Tyrosine Kinases Receptors FLT3, KIT and PDGFR-β, Exhibits Powerful In Vivo Anti-Glioblastoma Activity. *Cancers* **2020**, *12*, 3423. [CrossRef] [PubMed]
10. Ali, F.; S Hosmane, N.; Zhu, Y. Boron Chemistry for Medical Applications. *Molecules* **2020**, *25*, 828. [CrossRef]
11. Stockmann, P.; Gozzi, M.; Kuhnert, R.; Sárosi, M.B.; Hey-Hawkins, E. New keys for old locks: Carborane-containing drugs as platforms for mechanism-based therapies. *Chem. Soc. Rev.* **2019**, *48*, 3497–3512. [CrossRef]
12. Bogdanovic, B.; Schwickardi, M. Ti-doped alkali metal aluminium hydrides as potential novel reversible hydrogen storage materials. *J. Alloys Compd.* **1997**, *253–254*, 1–9. [CrossRef]
13. Yang, J.; Sudik, A.; Wolverton, C.; Siegel, D.J. High capacity hydrogen storage materials: Attributes for automotive applications and techniques for materials discovery. *Chem. Soc. Rev.* **2010**, *39*, 656–675. [CrossRef]
14. Bellosta von Colbe, J.; Ares, J.-R.; Barale, J.; Baricco, M.; Buckley, C.; Capurso, G.; Gallandat, N.; Grant, D.M.; Guzik, M.N.; Jacob, I.; et al. Application of hydrides in hydrogen storage and compression: Achievements, outlook and perspectives. *Int. J. Hydrog. Energy* **2019**, *44*, 7780–7808. [CrossRef]
15. Schneemann, A.; White, J.L.; Kang, S.; Jeong, S.; Wan, L.F.; Cho, E.S.; Heo, T.W.; Prendergast, D.; Urban, J.J.; Wood, B.C.; et al. Nanostructured Metal Hydrides for Hydrogen Storage. *Chem. Rev.* **2018**, *118*, 10775–10839. [CrossRef]
16. Ohno, S.; Banik, A.; Dewald, G.F.; Kraft, M.A.; Krauskopf, T.; Minafra, N.; Till, P.; Weiss, M.; Zeier, W.G. Materials design of ionic conductors for solid state batteries. *Prog. Energy* **2020**, *2*, 022001. [CrossRef]
17. Paskevicius, M.; Jepsen, L.H.; Schouwink, P.; Černý, R.; Ravnsbæk, D.B.; Filinchuk, Y.; Dornheim, M.; Besenbacher, F.; Jensen, T.R. Metal borohydrides and derivatives–synthesis, structure and properties. *Chem. Soc. Rev.* **2017**, *46*, 1565–1634. [CrossRef]
18. Černý, R.; Schouwink, P. The crystal chemistry of inorganic metal borohydrides and their relation to metal oxides. *Acta Cryst.* **2015**, *B71*, 619–640. [CrossRef]
19. Moussa, G.; Moury, R.; Demirci, U.B.; Sener, T.; Miele, P. Boron-based Hydrides for Chemical Hydrogen Storage. *Int. J. Energy Res.* **2013**, *37*, 825–842. [CrossRef]
20. Suárez-Alcántara, K.; Tena-Garcia, J.R.; Ricardo Guerrero-Ortiz, R. Alanates, a Comprehensive Review. *Materials* **2019**, *12*, 2724. [CrossRef]
21. Dobbins, T.A. Overview of the Structure–Dynamics–Function Relationships in Borohydrides for Use as Solid-State Electrolytes in Battery Applications. *Molecules* **2021**, *26*, 3239. [CrossRef] [PubMed]
22. Zavorotynska, O.; El-Kharbachi, A.; Deledda, S.; Hauback, B.C. Recent progress in magnesium borohydride $Mg(BH_4)_2$: Fundamentals and applications for energy storage. *Int. J. Hydrog. Energy* **2016**, *41*, 14387–14403. [CrossRef]
23. Zhang, Y.; Majzoub, E.; Ozoliņš, V.; Wolverton, C. Theoretical Prediction of Metastable Intermediates in the Decomposition of $Mg(BH_4)_2$. *J. Phys. Chem. C* **2012**, *116*, 10522–10528. [CrossRef]
24. Hwang, S.-J.; Bowman, R.C.; Reiter, J.W.; Rijssenbeek, J.; Soloveichik, G.L.; Zhao, J.-C.; Kabbour, H.; Ahn, C.C. NMR confirmation for formation of $[B_{12}H_{12}]^{2-}$ complexes during hydrogen desorption from metal borohydrides. *J. Phys. Chem. C* **2008**, *112*, 3164–3169. [CrossRef]
25. Golub, I.E.; Filippov, O.A.; Belkova, N.V.; Epstein, L.M.; Shubina, E.S. The Reaction of Hydrogen Halides with Tetrahydroborate Anion and Hexahydro-*closo*-hexaborate Dianion. *Molecules* **2021**, *26*, 3754. [CrossRef]
26. Voinova, V.V.; Selivanov, N.A.; Plyushchenko, I.V.; Vokuev, M.F.; Bykov, A.Y.; Klyukin, I.N.; Novikov, A.S.; Zhdanov, A.P.; Grigoriev, M.S.; Rodin, I.A.; et al. Fused 1,2-Diboraoxazoles Based on *closo*-Decaborate Anion–Novel Members of Diboroheterocycle Class. *Molecules* **2021**, *26*, 248. [CrossRef]
27. Andreichuk, E.P.; Anufriev, S.A.; Suponitsky, K.Y.; Sivaev, I.B. The First Nickelacarborane with *closo-nido* Structure. *Molecules* **2020**, *25*, 6009. [CrossRef]

28. Klyukin, I.N.; Vlasova, Y.S.; Novikov, A.S.; Zhdanov, A.P.; Hagemann, H.R.; Zhizhin, K.Y.; Kuznetsov, N.T. B-F bonding and reactivity analysis of mono- and perfluoro-substituted derivatives of closo-borate anions (6, 10, 12): A computational study. *Polyhedron* **2022**, *211*, 115559. [CrossRef]
29. Udovic, T.J.; Matsuo, M.; Unemoto, A.; Verdal, N.; Stavila, V.; Skripov, A.V.; Rush, J.J.; Takamura, H.; Orimo, S. Sodium Superionic Conduction in $Na_2B_{12}H_{12}$. *Chem. Commun.* **2014**, *50*, 3750–3752. [CrossRef]
30. Duchêne, L.; Remhof, A.; Hagemann, H.; Battaglia, C. Status and prospects of hydroborate electrolytes for all-solid-state batteries. *Energy Storage Mat.* **2020**, *26*, 543–549. [CrossRef]
31. He, L.; Li, H.-W.; Hwang, S.-J.; Akiba, E. Facile Solvent-Free Synthesis of anhydrous alkali metal dodecaborate $M_2B_{12}H_{12}$ (M = Li, Na, K). *J. Phys. Chem. C* **2014**, *118*, 6084–6089. [CrossRef]
32. Zhang, W.; Zhang, X.; Huang, Z.; Li, H.-W.; Gao, M.; Pan, H.; Liu, Y. Recent Development of Lithium Borohydride-Based Materials for Hydrogen Storage. *Adv. Energy Sustain. Res.* **2021**, *2*, 2100073. [CrossRef]
33. Filinchuk, Y.; Richter, B.; Jensen, T.R.; Dmitriev, V.; Chernyshov, D.; Hagemann, H. Porous and Dense Magnesium Borohydride Frameworks: Synthesis, Stability, and Reversible Absorption of Guest Species. *Angew. Chem. Int. Ed.* **2011**, *50*, 11162–11166. [CrossRef] [PubMed]
34. Yang, J.; Zhang, X.; Zheng, J.; Song, P.; Li, X. Decomposition pathway of $Mg(BH_4)_2$ under pressure: Metastable phases and thermodynamic parameters. *Scr. Mater.* **2011**, *64*, 225–228. [CrossRef]
35. Vitillo, J.G.; Bordiga, S.; Baricco, M. Spectroscopic and Structural Characterization of Thermal Decomposition of γ-$Mg(BH_4)_2$: Dynamic Vacuum versus H_2 Atmosphere. *J. Phys. Chem. C* **2015**, *119*, 25340–25351. [CrossRef]
36. Wang, X.; Xiao, X.; Zheng, J.; Yao, Z.; Zhang, M.; Huang, X.; Chen, L. Insights into magnesium borohydride dehydrogenation mechanism from its partial reversibility under moderate conditions. *Mater. Today Energy* **2020**, *18*, 100552. [CrossRef]
37. Crociani, L.; Rossetto, G.; Kaciulis, S.; Mezzi, A.; El-Habra, N.; Palmieri, V. Study of Magnesium Boride Films Obtained from $Mg(BH_4)_2$ by CVD. *Chem. Vap. Depos.* **2007**, *13*, 414–419. [CrossRef]
38. Kim, D.Y.; Yang, Y.; Abelson, J.R.; Girolami, G.S. Volatile magnesium octahydrotriborate complexes as potential CVD Precursors to MgB_2. Synthesis and Characterization of $Mg(B_3H_8)_2$ and its etherates. *Inorg. Chem.* **2007**, *46*, 9060–9066. [CrossRef]
39. Pistidda, C.; Garroni, S.; Dolci, F.; Gil Bardají, E.; Khandelwal, A.; Nolis, P.; Dornheim, M.; Gosalawit, R.; Jensen, T.; Cere-nius, Y.; et al. Synthesis of amorphous $Mg(BH_4)_2$ from MgB_2 and H_2 at room temperature. *J. Alloys Comp.* **2010**, *508*, 212–215. [CrossRef]
40. Severa, G.; Rönnebro, E.; Jensen, C.M. Direct hydrogenation of magnesium boride to magnesium borohydride: Demonstration of >11 weight percent reversible hydrogen storage. *Chem. Commun.* **2010**, *46*, 421–423. [CrossRef]
41. Sugai, C.; Kim, S.; Severa, G.; White, J.L.; Leick, N.; Martinez, M.B.; Gennett, T.; Stavila, V.; Jensen, C. Kinetic Enhancement of Direct Hydrogenation of MgB_2 to $Mg(BH_4)_2$ upon Mechanical Milling with THF, MgH_2, and/or Mg. *ChemPhysChem* **2019**, *20*, 1301–1304. [CrossRef]
42. Pistidda, C.; Santhosh, A.; Jerabek, P.; Shang, Y.; Girella, A.; Milanese, C.; Dore, M.; Garroni, S.; Bordignon, S.; Chierotti, M.R.; et al. Hydrogenation via a low energy mechanochemical approach: The MgB_2 case. *J. Phys. Energy* **2021**, *3*, 044001. [CrossRef]
43. Ray, K.G.; Klebanoff, L.E.; Lee, J.R.I.; Stavila, V.; Wook Heo, T.; Shea, P.; Baker, A.A.; Kang, S.; Bagge-Hansen, M.; Liu, Y.-S.; et al. Elucidating the mechanism of MgB_2 initial hydrogenation via a combined experimental–theoretical study. *Phys. Chem. Chem. Phys.* **2017**, *19*, 22646–22658. [CrossRef] [PubMed]
44. Chong, M.; Matsuo, M.; Orimo, S.; Autrey, T.; Jensen, C.M. Selective Reversible Hydrogenation of $Mg(B_3H_8)_2/MgH_2$ to $Mg(BH_4)_2$: Pathway to Reversible Borane-Based Hydrogen Storage? *Inorg. Chem.* **2015**, *54*, 4120–4125. [CrossRef]
45. Yue, Y.; Chen, L.; Peng, J. Thermal Behaviors and Their Correlations of $Mg(BH_4)_2$-Contained Explosives. *J. Energetic Mater.* **2018**, *36*, 82–92. [CrossRef]
46. Hagemann, H. Estimation of Thermodynamic Properties of Metal Hydroborates. *ChemistrySelect* **2019**, *4*, 8989–8992. [CrossRef]
47. Chase, M.W. NIST-JANAF Thermochemical Tables. *J. Phys. Chem. Ref. Data Monogr.* **1998**, *2*. [CrossRef]
48. Hagemann, H.; D'Anna, V.; Rapin, J.-P.; Yvon, K. Deuterium-Hydrogen Exchange in Solid $Mg(BH_4)_2$. *J. Phys. Chem. C* **2010**, *114*, 10045–10047. [CrossRef]
49. Sharma, M.; Sethio, D.; D'Anna, V.; Fallas, J.C.; Schouwink, P.; Cerný, R.; Hagemann, H. Isotope Exchange Reactions in $Ca(BH_4)_2$. *J. Phys. Chem. C* **2015**, *119*, 29–32. [CrossRef]
50. Huang, Z.; Wang, Y.; Wang, D.; Yang, F.; Wu, Z.; Wua, L.; Zhang, Z. Role of native defects and the effects of metal additives on the kinetics of magnesium borohydride. *Phys. Chem. Chem. Phys.* **2019**, *21*, 11226–11233. [CrossRef]
51. Heere, M.; Zavorotynska, O.; Deledda, S.; Sørby, M.H.; Book, D.; Steriotis, T.; Hauback, B.C. Effect of additives, ball milling and isotopic exchange in porous magnesium borohydride. *RSC Adv.* **2018**, *8*, 27645–27653. [CrossRef]
52. Li, H.W.; Kikuchi, K.; Nakamori, Y.; Miwa, K.; Towata, S.; Orimo, S. Effects of ball milling and additives on dehydriding behaviors of well-crystallized $Mg(BH_4)_2$. *Scr. Mater.* **2007**, *57*, 679–682. [CrossRef]
53. Saldan, I.; Frommen, C.; Llamas-Jansa, I.; Kalantzopoulos, G.N.; Hino, S.; Arstad, B.; Heyn, R.H.; Zavorotynska, O.; Deledda, S.; Sørby, M.H.; et al. Hydrogen storage properties of gamma-$Mg(BH_4)_2$ modified by MoO_3 and TiO_2. *Int. J. Hydrog. Energy* **2015**, *40*, 12286–12293. [CrossRef]
54. Chong, M.; Autrey, T.; Jensen, C.M. Lewis Base Complexes of Magnesium Borohydride: Enhanced Kinetics and Product Selectivity upon Hydrogen Release. *Inorganics* **2017**, *5*, 89. [CrossRef]

55. Dimitrievska, M.; Chong, M.; Bowden, M.E.; Wu, H.; Zhou, W.; Nayyar, I.; Ginovska, B.; Gennett, T.; Autrey, T.; Jensen, C.M.; et al. Structural and reorientational dynamics of tetrahydroborate (BH_4^-) and tetrahydrofuran (THF) in a $Mg(BH_4)_2 \cdot 3THF$ adduct: Neutron-scattering characterization. *Phys. Chem. Chem. Phys.* **2020**, *22*, 368–378. [CrossRef]
56. Tran, B.L.; Allen, T.N.; Bowden, M.E.; Autrey, T.; Jensen, C.M. Effects of Glymes on the Distribution of $Mg(B_{10}H_{10})$ and $Mg(B_{12}H_{12})$ from the Thermolysis of $Mg(BH_4)_2$. *Inorganics* **2021**, *9*, 41. [CrossRef]
57. Bell, R.T.; Strange, N.A.; Leick, N.; Stavila, V.; Bowden, M.E.; Autrey, T.S.; Gennett, T. $Mg(BH_4)_2$-Based Hybrid Metal–Organic Borohydride System Exhibiting Enhanced Chemical Stability in Melt. *ACS Appl. Energy Mater.* **2021**, *4*, 1704–1713. [CrossRef]
58. Wegner, W.; Jaroń, T.; Dobrowolski, M.A.; Dobrzycki, Ł.; Cyrańskic, M.K.; Grochala, W. Organic derivatives of Mg(BH4)2 as precursors towards MgB2 and novel inorganic mixed-cation borohydrides. *Dalton Trans.* **2016**, *45*, 14370–14377. [CrossRef]
59. Moury, R.; Gigante, A.; Remhof, A.; Roedern, E.; Hagemann, H. Experimental investigation of $Mg(B_3H_8)_2$ dimensionality, materials for energy storage applications. *Dalton Trans.* **2020**, *49*, 12168–12173. [CrossRef]
60. Gigante, A.; Leick, N.; Lipton, A.S.; Tran, B.; Strange, N.A.; Bowden, M.; Martinez, M.B.; Moury, R.; Gennett, T.; Hagemann, H.; et al. Thermal Conversion of Unsolvated $Mg(B_3H_8)_2$ to BH_4^- in the Presence of MgH_2. *ACS Appl. Energy Mater.* **2021**, *4*, 3737–3747. [CrossRef]
61. Newhouse, R.J.; Stavila, V.; Hwang, S.-J.; Klebanoff, L.E.; Zhang, J.Z. Reversibility and Improved Hydrogen Release of Magnesium Borohydride. *J. Phys. Chem. C* **2010**, *114*, 5224–5232. [CrossRef]
62. Beall, H.; Gaines, D.F. Mechanistic aspects of boron hydride reactions. *Inorg. Chim. Acta* **1999**, *289*, 1–10. [CrossRef]
63. Kurbonbekov, A.; Alikhanova, T.K.; Badalov, A.; Murufi, V.K.; Mirsaidov, U. Solubility in the lanthanum borohydride -potassium borohydride -tetrahydrofuran system at 25 °C and some thermodynamic characteristics of lanthanum borohydride. *Dokl. Akad. Nauk Tadzh. SSR* **1990**, *33*, 393–395.
64. Huang, Z.; Chen, X.; Yisgedu, T.; Meyers, E.A.; Shore, S.G.; Zhao, J.-C. Ammonium Octahydrotriborate ($NH_4B_3H_8$): New Synthesis, Structure, and Hydrolytic Hydrogen Release. *Inorg. Chem.* **2011**, *50*, 3738–3742. [CrossRef]
65. Good, W.D.; Mansson, M. The Thermochemistry of Boron and Some of Its Compounds. The Enthalpies of Formation of Orthoboric Acid, Trimethylamineborane, and Diammoniumdecaborane. *J. Phys. Chem.* **1966**, *70*, 97–104. [CrossRef]
66. Hanumantha Rao, M.; Muralidharan, K. closo-Dodecaborate $(B_{12}H_{12})^{2-}$ salts with nitrogen based cations and their energetic properties. *Polyhedron* **2016**, *115*, 105–110.
67. Dematteis, E.M.; Jensen, S.R.; Jensen, T.R.; Baricco, M. Heat capacity and thermodynamic properties of alkali and alkali-earth borohydrides. *J. Chem. Thermodyn.* **2020**, *143*, 106055. [CrossRef]
68. Pinatel, E.R.; Albanese, E.; Civalleri, B.; Baricco, M. Thermodynamic modelling of $Mg(BH_4)_2$. *J. Alloys Comp.* **2015**, *645*, S64–S68. [CrossRef]
69. Nguyen, M.T.; Matus, M.H.; Dixon, D.A. Heats of Formation of Boron Hydride Anions and Dianions and Their Ammonium Salts $[B_nH_m{}^{y-}][NH_4{}^+]_y$ with y = 1−2. *Inorg. Chem.* **2007**, *46*, 7561–7570. [CrossRef]
70. McKee, M.L. Estimation of Heats of Formation of Boron Hydrides from ab Initio Energies. *J. Phys. Chem.* **1990**, *94*, 435–440. [CrossRef]
71. Kelley, S.P.; McCrary, P.D.; Flores, L.; Garner, E.B.; Dixon, D.A.; Rogers, R.D. Structural and Theoretical Study of Salts of the $[B_9H_{14}]^-$ Ion: Isolation of Multiple Isomers and Implications for Energy Storage. *ChemPlusChem* **2016**, *81*, 922–925. [CrossRef]
72. Sethio, D.; Lawson Daku, L.M.; Hagemann, H.; Kraka, E. Quantitative Assessment of B–B–B, B–H_b–B, and B–H_t Bonds: From BH_3 to $B_{12}H_{12}{}^{2-}$. *ChemPhysChem* **2019**, *20*, 1967–1977. [CrossRef]
73. Maillard, R.; Sethio, D.; Hagemann, H.; Lawson Daku, L.M. Accurate Computational Thermodynamics Using Anharmonic Density Functional Theory Calculations: The Case Study of B−H Species. *ACS Omega* **2019**, *4*, 8786–8794. [CrossRef]
74. Yu, C.L.; Bauer, S.H. Thermochemistry of the boranes. *J. Phys. Chem. Ref. Data* **1998**, *27*, 807–835. [CrossRef]
75. Lee, T.B.; Mc Kee, M.L. Redox Energetics of Hypercloso Boron Hydrides B_nH_n (n = 6–13) and $B_{12}X_{12}$ (X = F, Cl, OH, and CH_3). *Inorg. Chem.* **2012**, *51*, 4205–4214. [CrossRef]
76. Lee, T.B.; Mc Kee, M.L. Dissolution Thermochemistry of Alkali Metal Dianion Salts (M_2X_1, M = Li^+, Na^+, and K^+ with X = $CO_3{}^{2-}$, $SO_4{}^{2-}$, $C_8H_8{}^{2-}$, and $B_{12}H_{12}{}^{2-}$). *Inorg. Chem.* **2011**, *50*, 11412–11422. [CrossRef]
77. Yan, Y.; Remhof, A.; Rentsch, D.; Züttel, A. The role of $MgB_{12}H_{12}$ in the hydrogen desorption process of $Mg(BH_4)_2$. *Chem. Commun.* **2015**, *51*, 700–702.
78. Yan, Y.; Remhof, A.; Rentsch, D.; Lee, Y.S.; Cho, Y.W.; Züttel, A. Is $Y_2(B_{12}H_{12})_3$ the main intermediate in the decomposition process of $Y(BH_4)_3$? *Chem. Commun.* **2013**, *49*, 5234–5236. [CrossRef]
79. Godfroid, R.A.; Hill, T.G.; Onak, T.P.; Shore, S.G. Formation of $[BH_3]^{2-}$ and $[B_2H_6]^{2-}$ From the Homogeneous Reduction of B_2H_6. *J. Am. Chem. Soc.* **1994**, *116*, 12107–12108. [CrossRef]
80. Hill, T.G.; Godfroid, R.A.; White III, J.P.; Shore, S.G. Reduction of borane THF by alkali metal (potassium, rubidium, cesium) and ytterbium mercury amalgams to form salts of octahydrotriborate(1-); a simple procedure for the synthesis of tetraborane(10). *Inorg. Chem.* **1991**, *30*, 2952–2954. [CrossRef]
81. Gaines, D.F.; Schaeffer, R.; Tebbe, F. Convenient Preparations of Solutions Containing the Triborohydride Ion. *Inorg. Chem.* **1963**, *2*, 526–528. [CrossRef]
82. Chen, X.; Liu, X.-R.; Wang, X.; Chen, X.-M.; Jing, Y.; Wie, D. A Safe and Efficient Synthetic Method of the Alkali Metal Octahydrotriborate, Unravelling a General Mechanism of Constructing the Delta B3 Unit of Polyhedral Boranes. *Dalton Trans.* **2021**, *50*, 13676–13679. [CrossRef]

83. Chen, X.-M.; Ma, N.; Zhang, Q.-F.; Wang, J.; Feng, X.; Wei, C.; Wang, L.-S.; Zhang, J.; Chen, X. Elucidation of the Formation Mechanisms of the Octahydrotriborate Anion ($B_3H_8^-$) through the Nucleophilicity of the B–H Bond. *J. Amer. Chem. Soc.* **2018**, *140*, 6718–6726. [CrossRef]
84. Moury, R.; Gigante, A.; Hagemann, H. An alternative approach to the synthesis of NaB_3H_8 and $Na_2B_{12}H_{12}$ for solid electrolyte applications. *Int. J. Hydrog. Energy* **2017**, *42*, 22417–22421. [CrossRef]
85. Grinderslev, J.B.; Møller, K.T.; Yan, Y.; Chen, X.-M.; Li, Y.; Li, H.-W.; Zhou, W.; Skibsted, J.; Chen, X.; Jensen, T.R. Potassium octahydridotriborate: Diverse polymorphism in a potential hydrogen storage material and potassium ion conductor. *Dalton Trans.* **2019**, *48*, 8872–8881. [CrossRef]
86. Gigante, A.; Duchêne, L.; Moury, R.; Pupier, M.; Remhof, A.; Hagemann, H. Direct solution–based synthesis of the $Na_4(B_{12}H_{12})(B_{10}H_{10})$ solid electrolyte. *ChemSusChem* **2019**, *12*, 4832–4837. [CrossRef]
87. Aniya, M. A chemical approach for the microscopic mechanism of fast ion transport in solids. *Solid State Ion.* **1992**, *50*, 125–129. [CrossRef]
88. Matsuo, M.; Nakamori, Y.; Orimo, S.; Maekawa, H.; Takamura, H. Lithium superionic conduction in lithium borohydride accompanied by structural transition. *Appl. Phys. Lett.* **2007**, *91*, 224103. [CrossRef]
89. Muetterties, E.L.; Balthis, J.H.; Chia, Y.T.; Knoth, W.H.; Miller, H.C. Chemistry of Boranes. VIII. Salts and Acids of $B_{10}H_{10}^{-2}$ and $B_{12}H_{12}^{-2}$. *Inorg. Chem.* **1964**, *3*, 444–451. [CrossRef]
90. Černý, R.; Brighi, M.; Murgia, F. The Crystal Chemistry of Inorganic Hydroborates. *Chemistry* **2020**, *2*, 805–826. [CrossRef]
91. Wu, H.; Tang, W.S.; Stavila, V.; Zhou, W.; Rush, J.J.; Udovic, T.J. Structural Behavior of $Li_2B_{10}H_{10}$. *J. Phys. Chem. C* **2015**, *119*, 6481–6487. [CrossRef]
92. Her, J.-H.; Yousufuddin, M.; Zhou, W.; Jalisatgi, S.S.; Kulleck, J.G.; Zan, J.A.; Hwang, S.-J.; Bowman, R.C.; Udovic, T.J. Crystal structure of $Li_2B_{12}H_{12}$: A possible intermediate species in the decomposition of $LiBH_4$. *Inorg. Chem.* **2008**, *47*, 9757–9759. [CrossRef]
93. Paskevicius, M.; Pitt, M.P.; Brown, D.H.; Sheppard, D.A.; Chumphongphan, S.; Buckley, C.E. First-order phase transition in the $Li_2B_{12}H_{12}$ system. *Phys. Chem. Chem. Phys.* **2013**, *15*, 15825–15828. [CrossRef] [PubMed]
94. Wu, H.; Tang, W.S.; Zhou, W.; Stavila, V.; Rush, J.J.; Udovic, T.J. The structure of monoclinic $Na_2B_{10}H_{10}$: A combined diffraction, spectroscopy, and theoretical approach. *Cryst. Eng. Comm.* **2015**, *17*, 3533–3540. [CrossRef]
95. Verdal, N.; Her, J.-H.; Stavila, V.; Soloninin, A.V.; Babanova, O.A.; Skripov, A.V.; Udovic, T.J.; Rush, J.J. Complex high-temperature phase transitions in $Li_2B_{12}H_{12}$ and $Na_2B_{12}H_{12}$. *J. Solid State Chem.* **2014**, *212*, 81–91. [CrossRef]
96. Wunderlich, J.A.; Lipscomb, W.N. Structure of $B_{12}H_{12}^{-2}$ ion. *J. Am. Chem. Soc.* **1960**, *82*, 4427–4428. [CrossRef]
97. Hofmann, K.; Albert, B. Crystal structures of $M_2[B_{10}H_{10}]$ (M = Na, K, Rb) via real space simulated annealing powder techniques. *Z. Kristall.* **2005**, *220*, 142–146. [CrossRef]
98. Bukovsky, E.V.; Peryshkov, D.V.; Wu, H.; Zhou, W.; Tang, W.S.; Jones, W.M.; Stavila, V.; Udovic, T.J.; Strauss, S.H. Comparison of the Coordination of $B_{12}F_{12}^{2-}$, $B_{12}Cl_{12}^{2-}$, and $B_{12}H_{12}^{2-}$ to Na+ in the Solid State: Crystal Structures and Thermal Behavior of $Na_2B_{12}F_{12}$,$Na_2(H_2O)_4B_{12}F_{12}$, $Na_2B_{12}Cl_{12}$, and $Na_2(H_2O)_6B_{12}Cl_{12}$. *Inorg. Chem.* **2017**, *56*, 4369–4379. [CrossRef] [PubMed]
99. Tiritiris, I.; Schleid, T. The Dodecahydro-closo-Dodecaborates $M_2[B_{12}H_{12}]$ of the Heavy Alkali Metals (M = K^+, Rb^+, NH_4^+, Cs^+) and their Formal Iodide Adducts M_3I $[B_{12}H_{12}]$ (= $MI{\cdot}M_2[B_{12}H_{12}]$). *Z. Anorg. Allg. Chem.* **2003**, *629*, 1390–1402. [CrossRef]
100. Guggenberger, L.J. Chemistry of boranes. XXXIII. The crystal structure of $Rb_2B_9H_9$. *Inorg. Chem.* **1968**, *7*, 2260–2264. [CrossRef]
101. Verdal, N.; Wu, H.; Udovic, T.J.; Stavila, V.; Zhou, W.; Rush, J.J. Evidence of a transition to reorientational disorder in the cubic alkali-metal dodecahydro-closo-dodecaborates. *J. Solid State Chem.* **2011**, *184*, 3110–3116. [CrossRef]
102. Moury, R.; Lodziana, Z.; Remhof, A.; Duchêne, L.; Roedern, E.; Gigante, A.; Hagemann, H. Pressure-induced phase transitions in $Na_2B_{12}H_{12}$, structural investigation on a candidate for solid-state electrolyte. *Acta Cryst. B* **2019**, *B75*, 406–413. [CrossRef]
103. Maekawa, H.; Matsuo, M.; Takamura, H.; Ando, M.; Noda, Y.; Karahashi, T.; Orimo, S. Halide-stabilized $LiBH_4$, a room-temperature lithium fast-ion conductor. *J. Am. Chem. Soc.* **2009**, 894–895. [CrossRef]
104. Gulino, V.; Brighi, M.; Dematteis, E.M.; Murgia, F.; Nervi, C.; Cerny, R.; Baricco, M. Phase Stability and Fast Ion Conductivity in the Hexagonal $LiBH_4$-LiBr-LiCl Solid Solution. *Chem. Mater.* **2019**, *31*, 5133–5144. [CrossRef]
105. Sadikin, Y.; Schouwink, P.; Brighi, M.; Łodziana, Z.; Cerný, R. Modified anion packing of $Na_2B_{12}H_{12}$ in close to room temperature superionic conductors. *Inorg. Chem.* **2017**, *56*, 5006–5016. [CrossRef]
106. Kim, S.; Oguchi, H.; Toyama, N.; Sato, T.; Takagi, S.; Otomo, T.; Arunkumar, D.; Kuwata, N.; Kawamura, J.; Orimo, S. A complex hydride lithium superionic conductor for high-energy-density all-solid-state lithium metal batteries. *Nat. Commun.* **2019**, *10*, 1081. [CrossRef]
107. Payandeh, S.H.; Rentsch, D.; Łodziana, Z.; Asakura, R.; Bigler, L.; Černý, R.; Battaglia, C.; Remhof, A. Nido-Hydroborate-Based Electrolytes for All-Solid-State Lithium Batteries. *Adv. Funct. Mater.* **2021**, *31*, 2010046. [CrossRef]
108. Brighi, M.; Murgia, F.; Łodziana, Z.; Schouwink, P.; Wołczyk, A.; Černý, R. A mixed anion hydroborate/carba-hydroborate as a room temperature Na ion solid electrolyte. *J. Power Sources* **2019**, *404*, 7–12. [CrossRef]
109. Duchêne, L.; Kühnel, R.-S.; Rentsch, D.; Remhof, A.; Hagemann, H.; Battaglia, C. A highly stable sodium solid-state electrolyte based on a dodeca/deca-borate equimolar mixture. *Chem. Commun.* **2017**, *53*, 4195–4198. [CrossRef]
110. Yoshida, K.; Sato, T.; Unemoto, A.; Matsuo, M.; Ikeshoji, T.; Udovic, T.J.; Orimo, S.I. Fast sodium ionic conduction in $Na_2B_{10}H_{10}$-$Na_2B_{12}H_{12}$ pseudo-binary complex hydride and application to a bulk-type all-solid-state battery. *Appl. Phys. Lett.* **2017**, *110*, 103901. [CrossRef]

111. Payandeh, S.H.; Asakura, R.; Avramidou, P.; Rentsch, D.; Łodziana, Z.; Černý, R.; Remhof, A.; Battaglia, C. Nido-Borate/Closo-borate mixed-anion electrolytes for all-solid-state batteries. *Chem. Mater.* **2020**, *32*, 1101–1110. [CrossRef]
112. Brighi, M.; Murgia, F.; Cerny, R. Closo-Hydroborate Sodium Salts as an Emerging Class of Room-Temperature Solid Electrolytes. *Cell Rep. Phys. Sci.* **2020**, *1*, 100217. [CrossRef]
113. Skripov, A.V.; Soloninin, A.V.; Babanova, O.A.; Skoryunov, R.V. Anion and Cation Dynamics in Polyhydroborate Salts: NMR Studies. *Molecules* **2020**, *25*, 2940. [CrossRef]
114. Lohstroh, W.; Heere, M. Structure and Dynamics of Borohydrides Studied by Neutron Scattering Techniques: A Review. *J. Phys. Soc. Jpn.* **2020**, *89*, 1–12. [CrossRef]
115. Duchêne, L.; Lunghammer, S.; Burankova, T.; Liao, W.-C.; Embs, J.P.; Coperet, C.; Wilkening, H.M.R.; Remhof, A.; Hagemann, H.; Battaglia, C. Ionic conduction mechanism in the $Na_2(B_{12}H_{12})_{0.5}(B_{10}H_{10})_{0.5}$ closo-borate solid-state electrolyte: Interplay of disorder and ion–ion interactions. *Chem. Mater.* **2019**, *31*, 3449–3460. [CrossRef]
116. Asakura, R.; Duchêne, L.; Kühnel, R.-S.; Remhof, A.; Hagemann, H.; Battaglia, C. Electrochemical Oxidative Stability of Hydroborate-Based Solid-State Electrolytes. *ACS Appl. Energy Mater.* **2019**, *2*, 6924–6930. [CrossRef]
117. Matsuo, M.; Orimo, S. Lithium Fast-Ionic Conduction in Complex Hydrides: Review and Prospects. *Adv. Energy Mater.* **2011**, *1*, 161–172. [CrossRef]
118. Duchêne, L.; Kühnel, R.-S.; Stilp, E.; Reyes, E.C.; Remhof, A.; Hagemann, H.; Battaglia, C. A Stable 3 V all-solid-state sodium-ion battery based on a closo -borate electrolyte. *Energy Environ. Sci.* **2017**, *10*, 2609–2615. [CrossRef]
119. Murgia, F.; Brighi, M.; Cerny, R. Room-temperature-operating Na-ion solid state-battery with complex hydride as electrolyte. *Electrochem. Comm.* **2019**, *106*, 106534. [CrossRef]
120. Asakura, R.; Reber, D.; Duchêne, L.; Payandeh, S.; Remhof, A.; Hagemann, H.; Battaglia, C. 4 V room-temperature all-solid-state sodium battery enabled by a passivating cathode/hydroborate solid electrolyte interface. *Energy Environ. Sci.* **2020**, *13*, 5048–5058. [CrossRef]